Heliyon 9 (2023) e22231

Contents lists available at ScienceDirect

Heliyon

journal homepage: www.cell.com/heliyon

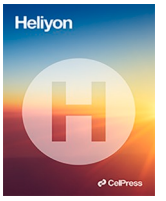

Numerical simulation of slug flow in pipelines using drift flux constitutive equations for gas-viscous oil two-phase flow

Victor Pugliese [a,b], Ana Buelvas [c], Oscar Pupo-Roncallo [b,*]

[a] Bob L. Herd Department of Petroleum Engineering, Texas Tech University, 79409, Lubbock, TX, United States
[b] Department of Mechanical Engineering, Universidad Del Norte, Km. 5 Vía a Puerto Colombia, Barranquilla, Colombia
[c] Department of Mechanical Engineering, Universidad Tecnológica de Bolívar. Parque Industrial y Tecnológico, Carlos Vélez Pombo, Km 1 Vía Turbaco, Cartagena, 130012, Colombia

ARTICLE INFO

Keywords:
Energy consumption
Pipe inclination
Liquid viscosity
Distribution coefficient
Gas drift velocity

ABSTRACT

Transient simulation of multiphase flow in pipes has been performed using Two-Fluid Model and Drift-Flux Model. The main advantage of the Drift-Flux Model is the reduced number of differential equations, which results in a lower computational time. However, the accuracy of the model depends on a suitable constitutive equation for the velocity of the dispersed phase, commonly, the gas phase. The gas velocity constitutive equation includes two important parameters, namely, the distribution coefficient and the void-fraction-weighted drift velocity.

A drift-flux-model code was developed, by using the Finite Volume Method (FVM) with staggered grid system, to evaluate the effect of highly viscous liquid and pipe geometry (pipe diameter and pipe inclination) in the prediction of liquid hold-up and pressure drop gradient. The gas phase compressibility was also included in the model.

The results show that the energy consumption to pump the fluids through the lift system has been overestimated when highly viscous liquids are produced. For the case of a vertical upward flow, the overestimation can be up to 10 % of energy consumption. We strongly recommend incorporating the effects of pipe inclination and liquid viscosity into the estimation of the Distribution Coefficient of the dispersed phase, encompassing both C_0 and gas drift velocity.

1. Introduction

Solving complex Computational Multi-Fluid Dynamic (CMFD) problems in engineering requires a multifaceted approach that spans various fields of study. Key to this endeavor is the selection of an appropriate multiphase flow model, typically comprising a system of partial differential equations derived from the fundamental principles of physics. Furthermore, choosing the most suitable computational model to approximate solutions is a critical step in this process. However, this decision is far from straightforward, especially considering the continuous evolution of computational models over the last four decades, with ongoing debates regarding their performance in terms of accuracy and convergence speed [1–5].

One of the key challenges in engineering is accurately calculating pressure drops in multiphase flows within pipelines, crucial for designing efficient thermo-fluid systems. To address this challenge, researchers have employed both empirical and mechanistic models [6–9]. These models are extensively used in computer simulations to optimize various systems. Empirical models, while practical,

* Corresponding author.
E-mail address: opupo@uninorte.edu.co (O. Pupo-Roncallo).

https://doi.org/10.1016/j.heliyon.2023.e22231
Received 13 July 2023; Received in revised form 23 September 2023; Accepted 7 November 2023
Available online 11 November 2023

often suffer from convergence issues due to the discontinuous nature of flow regime transitions. In contrast, mechanistic models, grounded in fundamental laws, offer smoother transitions in flow properties but face the limitation of fewer equations compared to the unknown variables inherent in multiphase flow situations [6,9–11]. To resolve this, constitutive equations or closure relationships are required to solve the system of equations.

Within engineering applications, slug flow is common in oil and gas transport operations, which are characterized by intermittent and unsteady behavior with the formation of bullet-shaped Taylor bubbles [12,13]. Understanding slug flow dynamics is pivotal in addressing a wide range of thermo-fluid challenges, such as paraffin or wax deposition [14,15], gas-liquid separation processes [16], and severe slugging in hilly terrain pipelines [17]. Quantifying slug size, frequency, and velocity plays an important role in predicting multiphase flow behavior, enabling the design and optimization of handling equipment.

In traditional multiphase flow models, it is accepted to assume that the distribution coefficient C_0 is approximately 2 for laminar flow within the slug body and around 1.2 for turbulent flow. These values are based on the theoretical ratio between maximum and average velocities in pipelines for each flow regime. However, this simplification fails to account for the influence of pipe inclination and the presence of high-viscosity liquids. To address these limitations, we have developed a drift-flux-model code utilizing the Finite Volume Method (FVM) with a staggered grid system [18,19]. This model aims to assess the impact of high-viscosity liquids and pipe geometry (including pipe diameter and inclination) on the prediction of liquid hold-up and pressure drop gradients, while also incorporating gas phase compressibility. The scope of this research is to evaluate the effect of pipe inclination and liquid viscosity on predicted gas fractions using a Drift Flux Model. It is important to note that this study does not aim to introduce a new numerical method; rather, it seeks to demonstrate how pressure drop calculations can be overestimated when commercial solvers rely on constitutive equations tailored for low-viscosity fluids, such as water, as is commonly seen in most works.

This paper is structured as follows: the remainder of Section 1 describes the Drift Flux Model and the constitutive equations employed. Section 2 provides insights into the numerical procedure used for simulating slug flow in inclined pipes with highly viscous liquids. Section 3 is dedicated to outlining the validation of the model. Section 4 presents and discusses the main results, and finally, Section 5 offers conclusions and recommendations drawn from this investigation.

1.1. One dimensional drift flux model

The theoretical framework used in this study is presented in Ref. [10]. The motion of the two-phase flow is expressed by the mixture-momentum equation and mass balance equation for the mixture and the dispersed phase. The following system of differential equations was obtained by averaging the local drift-flux formulation over the cross-sectional area,

$$\frac{\partial\langle\rho_m\rangle}{\partial t}+\frac{\partial(\langle\rho_m\rangle\overline{v_m})}{\partial x}=0 \tag{1}$$

$$\frac{\partial(\langle\alpha\rangle\rho_G)}{\partial t}+\frac{\partial(\langle\alpha\rangle\rho_G\overline{v_m})}{\partial x}=\Gamma_G-\frac{\partial}{\partial x}\left(\frac{\langle\alpha\rangle\rho_G\rho_L}{\langle\rho_m\rangle}\,\overline{V_{Gj}}\right) \tag{2}$$

$$\frac{\partial(\langle\rho_m\rangle\overline{v_m})}{\partial t}+\frac{\partial(\langle\rho_m\rangle\overline{v_m}^2)}{\partial x}+\frac{\partial p}{\partial x}=\langle\rho_m\rangle g_x+\langle\rho_m\rangle\frac{f_m}{2D}\,\overline{v_m}|\overline{v_m}|-\frac{\partial}{\partial x}\left[\frac{\langle\alpha\rangle\rho_G\rho_L}{(1-\langle\alpha\rangle)\langle\rho_m\rangle}\,\overline{V_{Gj}}^2\right] \tag{3}$$

where $\langle\rho_m\rangle[kg/m^3]$ is the mixture density and $\overline{v_m}[m/s]$ is the mixture velocity defined as

$$\langle\rho_m\rangle=\langle\alpha\rangle\rho_G+(1-\langle\alpha\rangle)\rho_L \tag{4}$$

$$\overline{v_m}=\frac{\langle\alpha\rangle\rho_G\langle\langle v_G\rangle\rangle+(1-\langle\alpha\rangle)\rho_L\langle\langle v_L\rangle\rangle}{\langle\rho_m\rangle} \tag{5}$$

where $\langle\langle v_G\rangle\rangle[m/s]$ and $\langle\langle v_L\rangle\rangle[m/s]$ are the mean gas and liquid velocities. The gas and liquid densities, $\rho_G[kg/m^3]$ and $\rho_L[kg/m^3]$, are considered constant within any cross-sectional area. Equations (1)–(3) are used to solve the gas volume fraction $\langle\alpha\rangle$, the mixture velocity $\overline{v_m}[m/s]$, and the pressure $p[Pa]$, as functions of position $x[m]$ and time $t[sec]$. $\Gamma_G[kg/m^3/s]$ is the gas volumetric generation rate and $g_x[m/s^2]$ is the gravity component along the pipe axis. The term represented by $\langle\rho_m\rangle f_m\,\overline{v_m}|\overline{v_m}|/(2D)$ in equation (3) is the two-phase frictional pressure drop.

The void-fraction-weighted gas velocity, $\langle\langle v_G\rangle\rangle[m/s]$, is modeled as:

$$\langle\langle v_G\rangle\rangle=\frac{\langle j_G\rangle}{\langle\alpha\rangle}=C_0\langle j\rangle+\langle\langle V_{Gj}\rangle\rangle \tag{6}$$

$$\langle j\rangle=\langle j_G\rangle+\langle j_L\rangle \tag{7}$$

The parameter C_0 is a distribution coefficient related to the velocity and concentration profiles in dispersed systems, $\langle j\rangle[m/s]$ is the average volumetric flux, $\langle\langle V_{Gj}\rangle\rangle[m/s]$ is the local gas drift velocity, and $\langle j_G\rangle[m/s]$ and $\langle j_L\rangle[m/s]$ are the gas and liquid superficial velocity, respectively. The effect of the relative velocities between the phases is included using the mean gas drift velocity concept, $\overline{V_{Gj}}[m/s]$. Once, the distribution coefficient C_0 and the local drift velocity $\langle\langle V_{Gj}\rangle\rangle$ are obtained, the mean drift velocity $\overline{V_{Gj}}$ is estimated using the following equation:

$$\overline{V_{Gj}} = \frac{\langle \rho_m \rangle \langle \langle V_{Gj} \rangle \rangle + (C_0 - 1)\langle \rho_m \rangle \overline{v_m}}{\langle \rho_m \rangle - (C_0 - 1)\langle \alpha \rangle (\rho_L - \rho_G)} \tag{8}$$

1.2. Drift flux model constitutive equations

1.2.1. Bendiksen [8]

Bendiksen [8] correlated the drift velocity for inclined flow by using the drift velocity for horizontal and vertical flow by:

$$\langle \langle V_{Gj} \rangle \rangle = (0.542 \cos\theta + 0.351 \sin\theta)\sqrt{gD} \tag{9}$$

The distribution coefficient C_0 depends on the Reynolds Number:

$$C_0 = \begin{cases} 2 & Re_j < 2,100 \\ 1.2 & Re_j \geq 2,100 \end{cases}, \tag{10a}$$

where Re_j is the two-phase mixture Reynolds Number, defined as follows:

$$Re_j = \rho_L \langle j \rangle D_H / \mu_L \tag{10b}$$

1.2.2. Bhagwat & Ghajar [20]

Bhagwat and Ghajar [20] proposed a gas volume fraction correlation that is independent of flow regime. The data base they used includes data from pipes with hydraulic diameters ranging from 0.5 to 305 mm, various pipe orientations within the range of $-90^\circ \leq \theta \leq 90^\circ$, and liquid viscosities spanning 0.001 to 0.6 $Pa \bullet s$.

The gas drift velocity $\langle \langle V_{Gj} \rangle \rangle$ is calculated as follows:

$$\langle \langle V_{Gj} \rangle \rangle = (0.35 \sin\theta + 0.45 \cos\theta)\sqrt{\frac{\Delta \rho g D_H}{\rho_L}}(1 - \langle \alpha \rangle)^{0.5} C_2 C_3 C_4 \tag{11}$$

where C_2, C_3, C_4 are parameter defined in Bhagwat and Ghajar (2014).

The distribution coefficient C_0 is estimated by the following equation:

$$C_0 = \frac{2 - (\rho_G/\rho_L)^2}{1 + \left(Re_j/1,000\right)^2} + \frac{\left[\left(1 + (\rho_G/\rho_L)^2 \cos\theta\right) \Big/ (1 + \cos\theta)\right]^{0.2(1-\langle \alpha \rangle)} + C_{0,1}}{1 + \left(1,000/Re_j\right)^2} \tag{12a}$$

$C_{0,1}$ is a function of the ratio of gas to liquid density ρ_G/ρ_L, gas volumetric flow fraction β, two-phase Fanning friction factor f_{tp}, and two-phase flow quality χ:

$$C_{0,1} = \left(C_1 - C_1\sqrt{\rho_G/\rho_L}\right)\left[(2.6 - \beta)^{0.15} - \sqrt{f_{tp}}\right](1 - \chi)^{1.5} \tag{12b}$$

where C_1 is assumed to be 0.2 for circular and annular pipes and 0.4 for rectangular pipes.

1.2.3. Pugliese et al. [18,19]

A new constitutive equation for gas drift velocity with high-viscosity liquid two-phase slug flow was presented by Pugliese et al. in Ref. [18], and its performance was compared with previous model. This model is based on 400 CFD simulations, and the data base includes cases with hydraulic pipe diameters in a range of 38–152 mm, pipe orientations in a range of $0^\circ \leq \theta \leq 90^\circ$, and liquid viscosities in a range of 0.14–1.12 $Pa \bullet s$. In this model, two independent dimensionless number, Eötvös Number E_o and Bouyancy Number N_f, are used to predict the Reynolds Number, which is based on the gas drift velocity:

$$\begin{aligned} Re_{Vd} = {} & a_0 + E_o(a_1 \sin\theta + a_2 \cos\theta) + N_f(a_3 \sin\theta + a_4 \cos\theta) \\ & + E_o^2(a_5 \sin\theta + a_6 \cos\theta) + N_f^2(a_7 \sin\theta + a_8 \cos\theta) \\ & + \sqrt{E_o}(a_9 \sin\theta + a_{10} \cos\theta) + \sqrt{N_f}(a_{11} \sin\theta + a_{12} \cos\theta) \end{aligned} \tag{13a}$$

$$E_o = (\rho_L - \rho_G) g D_H / \sigma \tag{13b}$$

$$N_f = \left[D_H^3 g(\rho_L - \rho_G)\rho_L\right]^{0.5} \Big/ \mu_L \tag{13c}$$

$$Re_{Vd} = \rho_L \langle \langle V_{Gj} \rangle \rangle D_H / \mu_L \tag{13d}$$

where the parameters a_i in equation (13) are defined in Pugliese et al. [19].

The distribution coefficient C_0 is given as follows,

$$C_0 = a_0 + \ln(Re_j)(a_1 \sin\theta + a_2 \cos\theta) + Fr_j(a_3 \sin\theta + a_4 \cos\theta) + (\ln Re_j)^2(a_5 \sin\theta + a_6 \cos\theta) + Fr_j^2(a_7 \sin\theta + a_8 \cos\theta) + (\ln Re_j)^3(a_9 \sin\theta + a_{10} \cos\theta) + Fr_j^3(a_{11} \sin\theta + a_{12} \cos\theta) \tag{14a}$$

$$Fr_j = \langle j \rangle \Big/ \sqrt{gD_H(1-\rho_G/\rho_L)} \tag{14b}$$

where Re_j is defined in equation (10b) and the parameters a_i in equation (14) are defined by Pugliese et al. in Ref. [19].

1.3. Frictional pressure drop

The term represented by $\langle \rho_m \rangle f_m \, \overline{v_m}|\overline{v_m}|/(2D)$ in equation (3) is the two-phase frictional pressure drop. The two-phase flow frictional pressure drop calculation is based on the two-phase Darcy-Weisbach friction multipliers, φ_L^2 and φ_G^2 [21],

$$\langle \rho_m \rangle \frac{f_m}{2D} \, \overline{v_m}|\overline{v_m}| = \left.\frac{dp}{dx}\right|_{two\ phase} \tag{15a}$$

$$\left.\frac{dp}{dx}\right|_{two\ phase} = \varphi_L^2 \left.\frac{dp}{dx}\right|_L = \varphi_G^2 \left.\frac{dp}{dx}\right|_G \tag{15b}$$

where $\left.\frac{dp}{dx}\right|_L$ and $\left.\frac{dp}{dx}\right|_G$ are the pressure gradient calculed assuming single phase flow.

2. Numerical method

2.1. Discretization schemes

The staggered mesh approach, with velocities defined at the mesh boundaries and pressure, gas volume fraction and fluid properties defined within the cells, is implemented for the spatial discretization of the differential equation system [22]. This approach allows avoiding the specification of an extra boundary condition because the convection term in the transport equation includes N faces (N velocity knowns) for the N cells, i.e., the upstream velocity is an inlet condition, and the outlet velocity is not required. Fig. 1 shows a representation of the staggered mesh used. It should be noted that the distribution coefficient C_0 and the local drift velocity $\langle\langle V_{Gj} \rangle\rangle$ are defined at the cell center because these parameters depend on the fluid properties.

All advection terms are discretized using the donor cell concept, which is a first order and stable discretization scheme. Table 1 shows the discretized advection terms. The superscript * refers to the following condition: if the mixture velocity at the interface is positive, the variables defined in the center of the cell are evaluated in the upstream cell. For example:

$$\left(\frac{\langle\alpha\rangle\rho_G\rho_L}{\langle\rho_m\rangle}\,\overline{V_{Gj}}\right)^*_{i+\frac{1}{2}} = \begin{cases} \left(\frac{\langle\alpha\rangle\rho_G\rho_L}{\langle\rho_m\rangle}\,\overline{V_{Gj}}\right)_i, & if\ V_{m,i+\frac{1}{2}} \geq 0 \\ \left(\frac{\langle\alpha\rangle\rho_G\rho_L}{\langle\rho_m\rangle}\,\overline{V_{Gj}}\right)_{i+1}, & if\ V_{m,i+\frac{1}{2}} < 0 \end{cases} \tag{16}$$

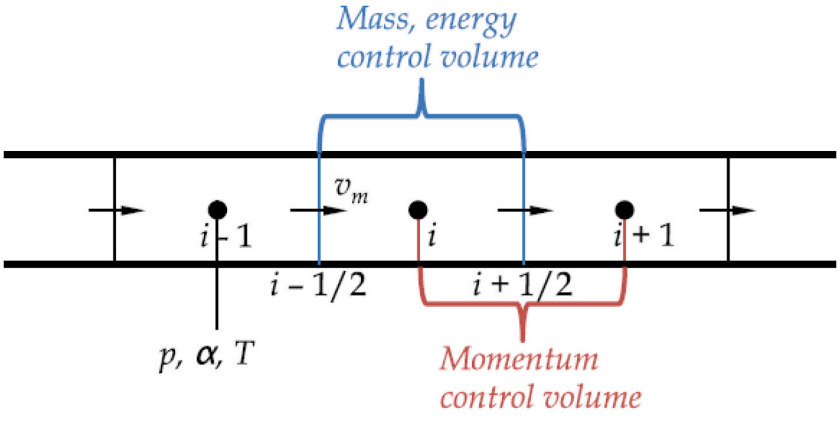

Fig. 1. Staggered mesh scheme, modified from Ref. [23].

Table 1
Discretization Schemes using Donor Cell Concept.

Advection Terms: Donor Cell Concept
$\frac{\partial(\langle\rho_m\rangle\overline{v_m})}{\partial x} = \frac{1}{\Delta x}\left[(\langle\rho_m\rangle^*\overline{v_m})_{i+\frac{1}{2}} - (\langle\rho_m\rangle^*\overline{v_m})_{i-\frac{1}{2}}\right]$
$\frac{\partial(\langle\alpha\rangle\rho_G\overline{v_m})}{\partial x} = \frac{1}{\Delta x}\left[(\langle\alpha\rangle^*\rho_G\overline{v_m})_{i+\frac{1}{2}} - (\langle\alpha\rangle^*\rho_G\overline{v_m})_{i-\frac{1}{2}}\right]$
$\frac{\partial}{\partial x}\left(\frac{\langle\alpha\rangle\rho_G\rho_L}{\langle\rho_m\rangle}\overline{V_{Gj}}\right) = \frac{1}{\Delta x}\left[\left(\frac{\langle\alpha\rangle\rho_G\rho_L}{\langle\rho_m\rangle}\overline{V_{Gj}}\right)^*_{i+\frac{1}{2}} - \left(\frac{\langle\alpha\rangle\rho_G\rho_L}{\langle\rho_m\rangle}\overline{V_{Gj}}\right)^*_{i-\frac{1}{2}}\right]$
$\frac{\partial(\langle\rho_m\rangle\overline{v_m}^2)}{\partial x} = \frac{1}{\Delta x}[\langle\rho_{m,i+1}\rangle\lvert\overline{v}_{m,i+1}\rvert(\overline{v}_{m,i+1})^* - \langle\rho_{m,i}\rangle\lvert\overline{v}_{m,i}\rvert(\overline{v}_{m,i})^*]$
$\frac{\partial}{\partial x}\left[\frac{\langle\alpha\rangle\rho_G\rho_L}{(1-\langle\alpha\rangle)\langle\rho_m\rangle}\overline{V_{Gj}}^2\right] = \frac{1}{\Delta x}\left[\left(\frac{\langle\alpha\rangle\rho_G\rho_L}{(1-\langle\alpha\rangle)\langle\rho_m\rangle}\overline{V_{Gj}}^2\right)_{i+1} - \left(\frac{\langle\alpha\rangle\rho_G\rho_L}{(1-\langle\alpha\rangle)\langle\rho_m\rangle}\overline{V_{Gj}}^2\right)_i\right]$

For time integration scheme, a semi-implicit method is used. Here we use the momentum balance equation, equation (3), as an example to summarize the discretized equations:

$$\frac{1}{\Delta t}\langle\rho_{m,i+\frac{1}{2}}\rangle^{n+1,*}\left(\overline{v}_{m,i+\frac{1}{2}}\right)^{n+1} + \frac{1}{\Delta x}\left[\langle\rho_{m,i+1}\rangle^n\lvert\overline{v}_{m,i+1}\rvert^n(\overline{v}_{m,i+1})^{n*} - \langle\rho_{m,i}\rangle^n\lvert\overline{v}_{m,i}\rvert^n(\overline{v}_{m,i})^{n*}\right] + \frac{1}{\Delta x}\left(p^{n+1}_{i+1} - p^{n+1}_i\right) + C^n = 0 \tag{17a}$$

$$C^n = -\frac{1}{\Delta t}\langle\rho_{m,i+\frac{1}{2}}\rangle^{n*}\left(\overline{v}_{m,i+\frac{1}{2}}\right)^n - (\langle\rho_m\rangle^* g_x)^n_{i+\frac{1}{2}} - \left(\langle\rho_m\rangle^*\frac{f_m}{2D}\lvert\overline{v}_m\rvert\overline{v}_m\right)^n_{i+\frac{1}{2}} + \frac{1}{\Delta x}\left[\left(\frac{\langle\alpha\rangle\rho_G\rho_L}{(1-\langle\alpha\rangle)\langle\rho_m\rangle}\overline{V_{Gj}}^2\right)_{i+1} - \left(\frac{\langle\alpha\rangle\rho_G\rho_L}{(1-\langle\alpha\rangle)\langle\rho_m\rangle}\overline{V_{Gj}}^2\right)_i\right]^n \tag{17b}$$

2.2. Boundary conditions

The boundary conditions at the inlet are:

$$\alpha(x=0) = \alpha_0(t) \tag{18a}$$

$$\overline{v}_m(x=0) = V_{m,0}(t) \tag{18b}$$

The boundary and numerical conditions at the outlet are:

$$P(x=L) = P_{outlet} \tag{19a}$$

$$\left.\frac{\partial\alpha}{\partial x}\right|_{x=L} = 0 \rightarrow \alpha_L = \alpha_{L+1}, \forall t \tag{19b}$$

$$\left.\frac{\partial\overline{v}_m}{\partial x}\right|_{x=L} = 0 \rightarrow V_{m,L+\frac{1}{2}} = V_{m,L+\frac{3}{2}}, \forall t \tag{19c}$$

2.3. Solution method: Pressure-implicit-split-operators (PISO) algorithm

In the following discussion, the superscript * refers to guessed variables. The discretized momentum equation is solved using the guessed pressure field, $\boldsymbol{p}^*$, to yield velocity field, $\overline{\boldsymbol{v}}^*_{\boldsymbol{m}}$:

$$\frac{1}{\Delta t}\langle\rho_{m,i+\frac{1}{2}}\rangle^{n+1}\left(\overline{\boldsymbol{v}}_{\boldsymbol{m},\boldsymbol{i}+\frac{1}{2}}\right)^* = -\frac{1}{\Delta x}\left[\langle\rho_{m,i+1}\rangle^n\lvert\overline{v}_{m,i+1}\rvert^n(\overline{v}_{m,i+1})^n - \langle\rho_{m,i}\rangle^n\lvert\overline{v}_{m,i}\rvert^n(\overline{v}_{m,i})^n\right] - \frac{1}{\Delta x}\left(\boldsymbol{p}^*_{\boldsymbol{i+1}} - \boldsymbol{p}^*_{\boldsymbol{i}}\right) - C^n \tag{20}$$

We now define the correction p' as the difference between the correct pressure field and the guessed pressure field, p^*. The same approach applies to velocity and density:

$$p^{n+1} = p^* + p' \tag{21a}$$

$$\overline{v}_{m,i+\frac{1}{2}}^{n+1} = \overline{v}_{m,i+\frac{1}{2}}^{*} + \overline{v}_{m,i+\frac{1}{2}}^{'} \tag{21b}$$

Subtracting equation (20) from (17):

$$\begin{gathered}\frac{1}{\Delta t}\langle\rho_{m,i+\frac{1}{2}}\rangle^{n+1}\left[\left(\overline{v}_{m,i+\frac{1}{2}}\right)^{n+1} - \left(\overline{v}_{m,i+\frac{1}{2}}\right)^{*}\right] = -\frac{1}{\Delta x}\left(\left(p_{i+1}^{n+1} - p_{i+1}^{*}\right) - \left(p_{i}^{n+1} - p_{i}^{*}\right)\right) \\ \frac{1}{\Delta t}\langle\rho_{m,i+\frac{1}{2}}\rangle^{n+1}\overline{v}_{m,i+\frac{1}{2}}^{'} = -\frac{1}{\Delta x}\left(p_{i+1}^{'} - p_{i}^{'}\right) \\ \overline{v}_{m,i+\frac{1}{2}}^{'} = -\frac{\Delta t\left(p_{i+1}^{'} - p_{i}^{'}\right)}{\Delta x\langle\rho_{m,i+\frac{1}{2}}\rangle^{n+1}}\end{gathered} \tag{22}$$

Equation (22) describes the corrections to be applied to the velocities. So far, we have only considered the momentum equation, but the velocity field is also subject to the constraint that should satisfy continuity equation (1):

$$\frac{\langle\rho_{m,i}\rangle^{n+1} - \langle\rho_{m,i}\rangle^{n}}{\Delta t} + \frac{1}{\Delta x}\left[\langle\rho_{m,i+\frac{1}{2}}\rangle^{n+1}\left(\overline{v}_{m,i+\frac{1}{2}}\right)^{n+1} - \langle\rho_{m,i-\frac{1}{2}}\rangle^{n+1}\left(\overline{v}_{m,i-\frac{1}{2}}\right)^{n+1}\right] = 0$$

Substitution of the corrected velocities of equations (19b) and (20):

$$\begin{gathered}\frac{\Delta t}{\Delta x^2}p_{i+1}^{'} - \frac{2\Delta t}{\Delta x^2}p_{i}^{'} + \frac{\Delta t}{\Delta x^2}p_{i-1}^{'} = \frac{\langle\rho_{m,i}\rangle^{*} - \langle\rho_{m,i}\rangle^{n}}{\Delta t} \\ + \frac{1}{\Delta x}\left[\langle\rho_{m,i+\frac{1}{2}}\rangle^{*}\overline{v}_{m,i+\frac{1}{2}}^{*} - \frac{1}{\Delta x}\langle\rho_{m,i-\frac{1}{2}}\rangle^{*}\overline{v}_{m,i-\frac{1}{2}}^{*}\right]\end{gathered} \tag{23}$$

Equation (23) represents the discretized continuity equation as an equation for pressure correction $p^{'}$. The right-hand side is the continuity imbalance arising from the incorrect velocity field, $\overline{v}_{m}^{*}$. Once the pressure correction field $p^{'}$ is known, the correct pressure and velocity fields may be obtained. The pressure correction equation is susceptible to divergence unless some under-relation is used during the iterative process, β_p.

$$\begin{gathered}p^{**} = p^{*} + \beta_p p^{'} \\ v_{m,i+\frac{1}{2}}^{**} = \beta_v\left[v_{m,i+\frac{1}{2}}^{*} - \frac{\Delta t\left(p_{i+1}^{'} - p_{i}^{'}\right)}{\Delta x\left(\rho_{m,i+\frac{1}{2}}\right)^{n}}\right]^{n+1} + (1-\beta_v)\left[v_{m,i+\frac{1}{2}}\right]^{n}\end{gathered} \tag{24}$$

in summary, the PISO algorithm implemented includes the following steps.

i. Guess a pressure field, p^{*} (usually the pressure field at time n).
ii. Predict the gas void fraction field at time $n+1$, using an explicit formulation for equation (2). A CFL [24] condition of 0.25 was selected to guarantee the stability of the solver.
iii. Mixture density ρ_m^{n+1} is calculated by equation (4).
iv. **Predictor step**: $\overline{v}_m^{*}$ is predicted by equation (20).
v. **Corrector Step 1:** Pressure correction $p^{'}$ and velocity correction $\overline{v}_m^{'}$ are calculated by equations (21) and (20), respectively. Then, new corrected values for the pressure field p^{**} and velocity field $\overline{v}_m^{**}$ are estimated with equation (22).
vi. **Corrector Step 2:** A second correction is performed using equations (21) and (20), using as inputs p^{**} and $\overline{v}_m^{**}$. As results, $p^{''}$ and $\overline{v}_m^{''}$ are used to predict the values for pressure and velocity fields in time $n+1$.

3. Model validation

3.1. Water faucet problem

The water faucet problem was originally proposed by Ransom [25]. It is used for the purposes of code assessment, benchmark, and numerical verification for the two-phase drift flux model described in Sections 1 and 2. The problem consists of a vertical pipe of 12 m length and 1 m diameter. Initially, the pipe is filled with a uniform column of water moving with initial velocity $\langle\langle v_{L0}\rangle\rangle = 10m/s$ and a static gas annulus, and the cross-section average gas volume fraction is $\langle\alpha_0\rangle = 0.2$ for all the length. At the inlet, the liquid velocity $\langle\langle v_{L,i}\rangle\rangle = 10m/s$, while the gas velocity $\langle\langle v_{G,i}\rangle\rangle = 0$. The pressure at the bottom outlet is $p = 10^5 Pa$. A schematic representation is shown in Fig. 2.

The water faucet problem assumes no wall friction and not interfacial tension between the faces, then the analytical solution for the transient and steady state condition can be established.

$$\langle\langle v_L\rangle\rangle(x,t) = \begin{cases} \sqrt{\langle\langle v_{L,i}\rangle\rangle^2 + 2|g|x} & if\ x \le x_d \\ \langle\langle v_{L0}\rangle\rangle + gt & if\ x > x_d \end{cases} \tag{23a}$$

$$x_d = \langle\langle v_{L,i}\rangle\rangle t + \frac{gt^2}{2} \tag{23b}$$

$$\langle\alpha\rangle(x,t) = \begin{cases} 1 - (1-\langle\alpha_i\rangle)\langle\langle v_{L,i}\rangle\rangle \Big/ \sqrt{\langle\langle v_{L,i}\rangle\rangle^2 + 2|g|x} & if\ x \le x_d \\ \langle\alpha_0\rangle & if\ x > x_d \end{cases} \tag{24}$$

where x_d is the position of the gas volume fraction discontinuity. At the steady state condition, the solution yields to:

$$\langle\langle v_L\rangle\rangle(x) = \sqrt{\langle\langle v_{L,i}\rangle\rangle^2 + 2|g|x} \tag{25}$$

$$\langle\alpha\rangle(x) = 1 - \frac{(1-\langle\alpha_i\rangle)\langle\langle v_{L,i}\rangle\rangle}{\sqrt{\langle\langle v_{L,i}\rangle\rangle^2 + 2|g|x}} \tag{26}$$

Table 2 presents the parameters used for the water faucet problem. Also, the initial and boundary conditions required to validate the numerical solver.

3.2. Model validation

Mesh refinement study was performed for different numbers of cells, ranging from 50 to 400, equally spaced along the length of the pipe. Equations (25) and (26) are used as reference solution. The results of the mesh convergence studies are summarized in Table 3. In this table, $e_{\|L_1\|}$ correspond to the error base in the L_1 norm definition. From this table, we can conclude that the spatial discretization used in this model has a first-order accuracy.

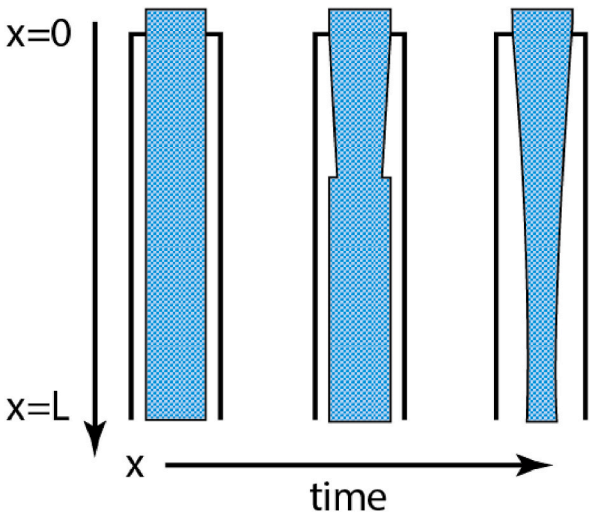

Fig. 2. Two-phase water faucet problem, modified from Ref. [23].

Table 2
Parameters, initial and boundary conditions for water faucet problem.

Parameter	Value
Pipe Length [m]	12
Gravity [m/s^2]	9.81
Initial Liquid Velocity $\langle\langle v_{L0}\rangle\rangle$ [m/s]	10
Initial Gas Velocity $\langle\langle v_{G0}\rangle\rangle$ [m/s]	0
Initial Gas Volume Fraction $\langle\alpha_0\rangle$	0.2
Initial Pressure [Pa]	10^5
Inlet Liquid Velocity $\langle\langle v_{L,i}\rangle\rangle$ [m/s]	10
Inlet Gas Velocity $\langle\langle v_{G,i}\rangle\rangle$ [m/s]	0
Inlet Gas Volume Fraction $\langle\alpha_i\rangle$	0.2
Outlet Pressure [Pa]	10^5

The numerical simulation results for the steady state condition are plotted against the Ransom analytical solution in Figs. 3 and 4. The numerical results accurately overlap with the analytical solution.

As the simulation starts, there is a gas volume fraction discontinuity moving downstream due to the gravity driving force. Fig. 5 shows the position of the gas volume fraction at time 0.5 s. As the mesh resolution increases, the numerical solution approaches the analytical solution. The numerical method is stable if the CFL condition is fulfilled; however, increasing the number of cells will increase the computation time.

4. Liquid viscosity effect on multi-phase slug flow in highly inclined pipes

4.1. Simulation cases

The model presented in Sections 1 and 3, including the drift flux constitutive equations for highly viscous liquids, is used to evaluate the effect of the liquid viscosity and pipe inclination on the pressure drop calculation in pipes. The inclinations of the pipe range from 0° (horizontal) to 90° (upward vertical), while the liquid viscosity range from 0.001 $Pa \bullet s$ to 1 $Pa \bullet s$. A total of 168 numerical experiments were carried out. The combination of experimental factors with the corresponding levels are presented in Table 4.

The flow condition remains consistent across all simulations. Initially, the pipe is filled with gas under static conditions, after which the gas phase begins to flow. The gas mass flow rate reaches its maximum value 100 s from the start of the simulation. For the subsequent 100 s, the gas mass flow rate remains constant until liquid enters the pipe. The maximum liquid mass flow rate is achieved at 300 s into the simulation. The simulation continues until the system reaches a steady-state condition. The maximum liquid mass flow rate is 0.1412 kg/s and the maximum gas mass flow rate is 0.001173 kg/s.

The computational domain consists of a 40 m length and 0.103 m ID pipe, and the mesh spacing Δx is 0.25 m uniformly distributed. Time step is selected accordingly to fulfil the CFL constrain.

4.2. Effect of liquid viscosity

Fig. 6 shows in the horizontal axis the liquid viscosity and, at the vertical axis, the gas volume $\langle\alpha\rangle$ fraction along the pipe predicted by solving the system of equations (1)–(3) using Bendiksen [8] and Pugliese et al. [18,19] models. The gas volume fraction is a cross-section averaged value. $\langle\alpha\rangle$. This is constant along the pipe if the pipe inclination is maintained constant. Bendiksen [8] model does not take into consideration the liquid viscosity. Because of this, for each pipe inclination the plots are horizontal and have a constant value for the gas volume fraction predicted. For slightly incline pipes, the mean drift velocity is low and the difference between both drift flux parameter models is negligible. However, when the pipe is highly inclined, such in the case of offshore risers, the average gas volume fraction could be 0.1 higher for highly viscous liquid two-phase flow.

The pressure drop gradient due to gravity is proportional to the mixture density, and according to equation (4), an increment of $\langle\alpha\rangle$ reduces the mixture density. Thus, the energy consumption to pump the fluids thought the lift system has been overestimated when highly viscous liquids are produced, and commercial software uses low viscosity liquid constitutive equations. For example, for the

Table 3
Mesh convergence study.

N_{cell}	$\Delta x[m] = L/N_{cell}$	$\Delta t[s]$	$\langle\langle v_L\rangle\rangle\left[\frac{m}{s}\right]$	
			$e_{\|L_1\|}$	Convergence Rate
50	0.24	0.003	0.08375	–
100	0.12	0.0015	0.05726	0.548
150	0.08	0.001	0.04433	0.631
200	0.06	0.00075	0.03622	0.702
400	0.03	0.000375	0.02053	0.819

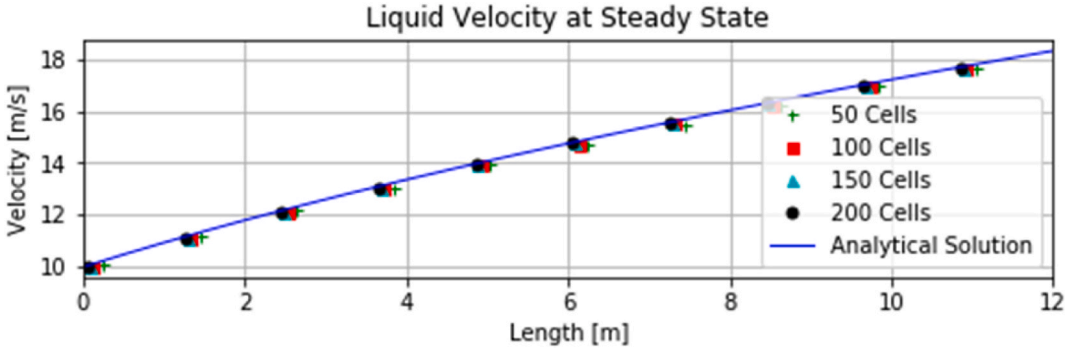

Fig. 3. Liquid velocity at the steady state for different number of cells.

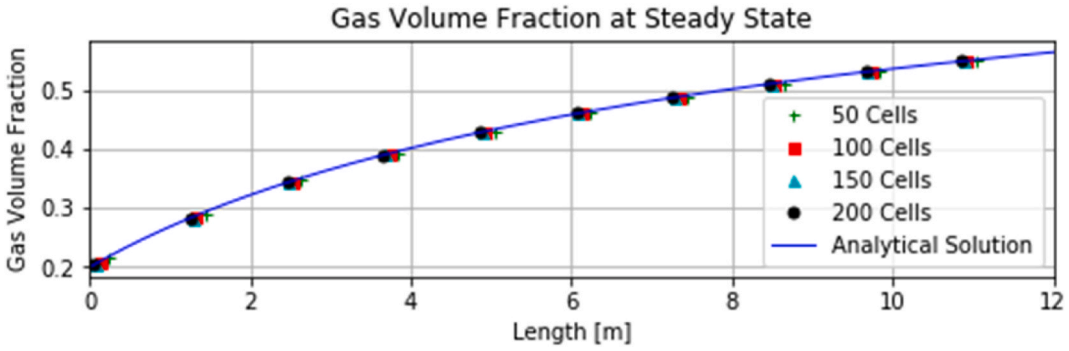

Fig. 4. Gas volume fraction at the steady state for different number of cells.

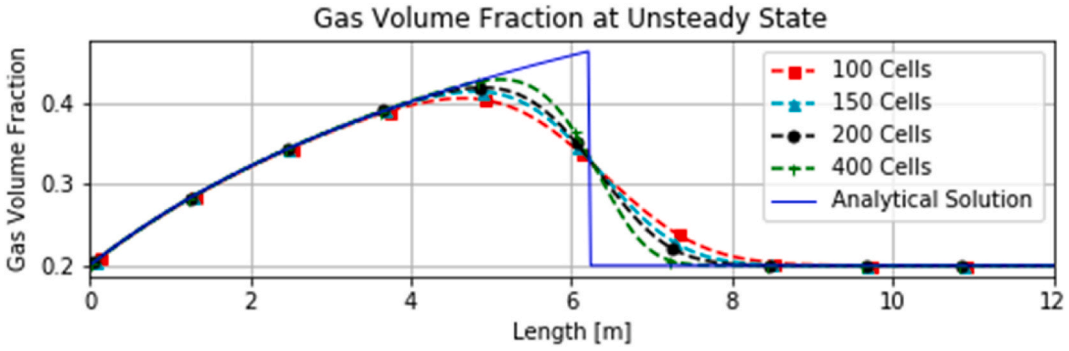

Fig. 5. Gas Volume Fraction discontinuity at time 0.5 s.

Table 4
Experimental factors.

Experiment Factors	Levels							
Liquid Viscosity [Pa.s]	0.001	0.05	0.1	0.2	0.4	0.6	0.8	1.0
Pipe Inclination [°]	0	15	30	45	60	75	90	
Drift Flux Parameters Model	Bendiksen [8]			Bhagwat and Ghajar [20]			Pugliese et al. [8,18]	

case of a vertical upward flow (90°), the overestimation can be up to 10 % of the energy consumption because the difference between gas volume fraction is 0.1 approximately.

For the calculation of pressure drop due to friction, the liquid viscosity has been included traditionally in the two-phase friction factor, but not in the mixture density. We strongly recommend incorporating the effects of pipe inclination and liquid viscosity into the estimation of the Distribution Coefficient of the dispersed phase, encompassing both C_0 and gas drift velocity.

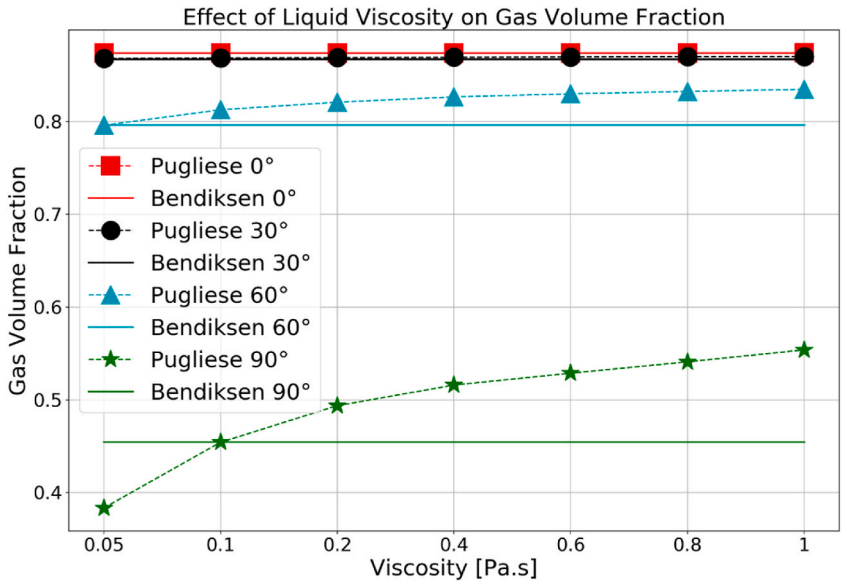

Fig. 6. Effect of liquid viscosity and pipe inclination on gas volume fraction $\langle\alpha\rangle$ prediction.

4.3. Comparison between bhagwat et al. [20] And pugliese et al. [18]

The comparison between the gas volume fraction predicted by Bhagwat and Ghajar [20] and Pugliese et al. [18] models is presented in Fig. 7. For slightly inclined pipe the difference is negligible, however, as the inclination increases the predicted gas volume fraction difference could be up to 0.2. Bhagwat and Ghajar [20] model is based on a data base which includes experimental data with hydraulic pipe diameters in a range of 0.5–305 mm, pipe orientations in a range of $-90^{\circ} \leq \theta \leq 90^{\circ}$, and liquid viscosity in a range of 0.001–0.6 $Pa \bullet s$. Pugliese et al. [18] model is based on 400 CFD simulations, and the data base includes cases with hydraulic pipe diameters in a range of 38–152 mm, pipe orientations in a range of $0^{\circ} \leq \theta \leq 90^{\circ}$, and liquid viscosity in a range of 0.14–1.12 $Pa \bullet s$. To evaluate the performance of both, it is recommended that an independent set of experiments should be conducted.

From the point of view of the numerical method, Bhagwat and Ghajar [20] model is implicit for the Distribution Coefficient C_0. This induces instabilities in the numerical method and more computational time if the initial guess for C_0 is not close to the final value. In contrast, Pugliese et al. [18] model is explicit for the distribution coefficient C_0 and the gas drift velocity $\langle\langle V_{Gj}\rangle\rangle$.

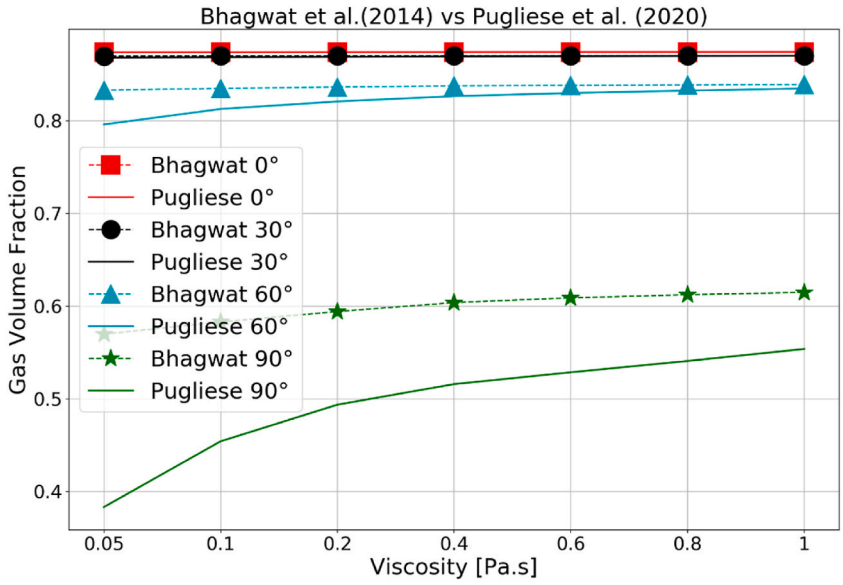

Fig. 7. Comparison between Bhagwat et al. [20] model and Pugliese et al. [18] model based on Gas Volume Fraction $\langle\alpha\rangle$ Prediction.

5. Conclusions and Recomendations

- Accurate prediction of distribution coefficient and gas drift velocity is important in gas-liquid two-phase flow system. These two-drift flux parameters impact the gas volume fraction prediction. Thus, the energy consumption to pump the fluids thought the lift system has been overestimated when highly viscous liquids are produced. For example, for the case of a vertical upward flow, the overestimation can be up to 10 % of the energy consumption.
- The effect of liquid viscosity for slightly inclined pipes on the gas volume fraction is negligible. However, for highly incline pipes the pressure drop due to gravity is strongly affected by the liquid viscosity. For gas lifting of highly viscous liquid, the bottom-hole pressure is overestimated with the current model used in commercial multiphase flow programs.
- To evaluate the performance of Bhagwat and Ghajar [20] and Pugliese et al. [18] models, it is recommended to conduct an independent set of experiments. However, in terms of the numerical method, the Pugliese et al. [18] model provides a faster solution.
- The PISO algorithm, described in Section 2.3, is suitable to solve a two-phase flow problem.

Ethical approval

This article does not contain any studies with human participants or animals performed by any of the authors.

Funding

The authors gratefully acknowledge Universidad del Norte, Colombia (Contract Identification: CCBUNDDA/12/2016) for the financial support. This research was also supported by the Fundación CEIBA - Gobernación de Bolívar through the program “Bolivar gana con ciencia”.

CRediT authorship contribution statement

Victor Pugliese: Conceptualization, Data curation, Formal analysis, Funding acquisition, Investigation, Methodology, Validation, Visualization, Writing – original draft. **Ana Buelvas:** Formal analysis, Investigation, Methodology, Writing – review & editing. **Oscar Pupo-Roncallo:** Formal analysis, Funding acquisition, Investigation, Methodology, Writing – review & editing.

Declaration of competing interest

The authors declare that they have no known competing financial interests or personal relationships that could have appeared to influence the work reported in this paper.

Nomenclature

A	*Pipe cross-section area* m^2
C_0	*Velocity Profile Distribution Coefficient*
D	*Inner Diameter of the pipe* m
Eo	*E öt v ös number*
Fr	*Froude Number*
Fr_j	*Froude Number based on an average volumetric flux*
$f_{\sigma i}$	*Interfacial Tension Force* Pa/m
g_i	*Gravitational Acceleration Vector* m/s^2
I	*Turbulence Intensity*
k	*Turbulent Kinetic Energy* J/kg
j	*Volumetric Flux* m/s
j_G	*Superficial Gas Velocity* m/s
j_L	*Superficial Liquid Velocity* m/s
L_{hy}	*Hydrodynamic Entrance Length* m
p	*Pressure* Pa
P_0	*Atmospheric Pressure* Pa
Re	*Reynolds Number*
Re_j	*Reynolds Number in the slug body*
R_t	*Dimensionless bubble tip radial position measured from the center of the pipe* m
t	*Time* s
u_i	*Velocity Vector* m/s
V	*Mean Flow Velocity* m/s
V_d	*Taylor Bubble Drift Velocity* m/s
v_G	*Gas Velocity* m/s

V_{Gj}	*Gas Drift Velocity* m/s
v_L	*Liquid Velocity* m/s
v_m	*Mixture Velocity* m/s
We	*Weber Number*
$We_{V_{Gj}}$	*Weber Number for a bubble in stagnant fluid*
x_i	*Position Vector* m

Greek Symbols

α	*Local Gas Volume Fraction*
α_c	*Gas Volume Fraction close to the pipe axis*
α_w	*Gas Volume Fraction close to the pipe wall*
Δ	*Turbulent Length Scale or Filter-Width Scale* m
θ	*Inclination Angle of the Pipe from the horizontal axis* rad
κ	*Interface curvature* m^{-1}
μ_G	*Viscosity of Gas phase* $Pa \bullet s$
μ_L	*Viscosity of Liquid phase* $Pa \bullet s$
μ_m	*Viscosity of the Mixture* $Pa \bullet s$
μ_t	*Turbulent or Eddy viscosity* $Pa \bullet s$
ρ_G	*Density of Gas phase* kg/m^3
ρ_L	*Density of Liquid phase* kg/m^3
ρ_m	*Density of the Mixture* kg/m^3
σ	*Interfacial tension constant* N/m

Mathematical Symbols

$\partial\bullet$	*Partial Derivative*
$\overline{\bullet}$	*Time average*
$\nabla\bullet$	*Gradient Operator*
$(\bullet)^T$	*Transpose Operator*
$\mathrm{tr}(\bullet)$	*Trace Operator*
$\mathrm{dev}(\bullet)$	*Deviatoric Component of a matrix*
$\langle \bullet \rangle$	*Cross-sectional area average*
$\langle\langle \bullet \rangle\rangle$	*Void fraction weighted variable*

References

[1] A.M. Davies, C. V Stephens, Comparison of the finite difference and Galerkin methods as applied to the solution of the hydrodynamic equations, Appl. Math. Model. 7 (1983) 226–240, https://doi.org/10.1016/0307-904X(83)90076-8.

[2] R. Garg, C. Narayanan, D. Lakehal, S. Subramaniam, Accurate numerical estimation of interphase momentum transfer in Lagrangian–Eulerian simulations of dispersed two-phase flows, Int. J. Multiphas. Flow 33 (2007) 1337–1364, https://doi.org/10.1016/j.ijmultiphaseflow.2007.06.002.

[3] D.O. Njobuenwu, M. Fairweather, J. Yao, Coupled RANS–LPT modelling of dilute, particle-laden flow in a duct with a 90° bend, Int. J. Multiphas. Flow 50 (2013) 71–88, https://doi.org/10.1016/j.ijmultiphaseflow.2012.10.009.

[4] A.V. Farahani, M. Montazeri, Computational method for multiphase flow characterization in the gas refinery, Heliyon 6 (2020), e03193, https://doi.org/10.1016/j.heliyon.2020.e03193.

[5] J. López, N. Ratkovich, E. Pereyra, Analysis of two-phase air-water annular flow in U-bends, Heliyon 6 (2020), e05818, https://doi.org/10.1016/j.heliyon.2020.e05818.

[6] A.E. Dukler, M.G. Hubbard, A model for gas-liquid slug flow in horizontal and near horizontal tubes, Ind. Eng. Chem. Fundam. 14 (1975) 337–347, https://doi.org/10.1021/i160056a011.

[7] M. Ishii, One-dimensional Drift-Flux Model and Constitutive Equations for Relative Motion between Phases in Various Two-phase Flow Regimes, United States, 1977, https://doi.org/10.2172/6871478.

[8] K.H. Bendiksen, An experimental investigation of the motion of long bubbles in inclined tubes, Int. J. Multiphas. Flow 10 (1984) 467–483, https://doi.org/10.1016/0301-9322(84)90057-0.

[9] O. Shoham, Mechanistic Modeling of Gas-Liquid Two-phase Flow in Pipes, Society of Petroleum Engineers, 2006, https://doi.org/10.2118/9781555631079.

[10] M. Ishii, T. Hibiki, Thermo-Fluid Dynamics of Two-phase Flow, Springer New York, New York, NY, 2011, https://doi.org/10.1007/978-1-4419-7985-8.

[11] R.A. Eghorieta, T.A. Afolabi, E. Panacharoensawad, Drift flux modeling of transient high-viscosity-liquid and gas two-phase flow in horizontal pipes, J. Pet. Sci. Eng. 171 (2018) 605–617, https://doi.org/10.1016/j.petrol.2018.07.047.

[12] B. Gokcal, A.S. Al-Sarkhi, C. Sarica, Effects of high oil viscosity on drift velocity for horizontal and upward inclined pipes, SPE projects, Facilities & Construction 4 (2009) 32–40, https://doi.org/10.2118/115342-PA.

[13] M. Ballesteros Martínez, E. Pereyra, N. Ratkovich, CFD study and experimental validation of low liquid-loading flow assurance in oil and gas transport: studying the effect of fluid properties and operating conditions on flow variables, Heliyon 6 (2020), e05705, https://doi.org/10.1016/j.heliyon.2020.e05705.

[14] C. Sarica, E. Panacharoensawad, Review of paraffin deposition research under multiphase flow conditions, Energy Fuel. 26 (2012) 3968–3978, https://doi.org/10.1021/ef300164q.

[15] A. Rittirong, E. Panacharoensawad, C. Sarica, Experimental study of paraffin deposition under two-phase gas/oil slug flow in horizontal pipes, SPE Prod. Oper. 32 (2017) 99–117, https://doi.org/10.2118/184386-PA.

[16] I. Karmon, E. Panacharoensawad, M. Watson, Quantifying a new horizontal well gas anchor performance, in: Day 1 Tue, SPE, 2019, https://doi.org/10.2118/195198-MS. April 09, 2019.

[17] R. Malekzadeh, R.A.W.M. Henkes, R.F. Mudde, Severe slugging in a long pipeline–riser system: experiments and predictions, Int. J. Multiphas. Flow 46 (2012) 9–21, https://doi.org/10.1016/j.ijmultiphaseflow.2012.06.004.
[18] V. Pugliese, A. Ettehadtavakkol, E. Panacharoensawad, Drift flux model parameters estimation based on numerical simulation of slug flow regime with high viscosity liquids in pipelines, Int. J. Multiphas. Flow 135 (2021), 103527, https://doi.org/10.1016/j.ijmultiphaseflow.2020.103527.
[19] V. Pugliese, E. Panacharoensawad, A. Ettehadtavakkol, Numerical study of the motion of a single elongated bubble in high viscosity stagnant liquids along pipelines, J. Pet. Sci. Eng. 190 (2020), 107088, https://doi.org/10.1016/j.petrol.2020.107088.
[20] S.M. Bhagwat, A.J. Ghajar, A flow pattern independent drift flux model based void fraction correlation for a wide range of gas–liquid two phase flow, Int. J. Multiphas. Flow 59 (2014) 186–205, https://doi.org/10.1016/j.ijmultiphaseflow.2013.11.001.
[21] K. Umminger, F. D'Auria, Pressure drops in nuclear thermal-hydraulics: principles, experiments, and modeling, in: F. D'Auria (Ed.), Thermal-hydraulics of Water Cooled Nuclear Reactors, Woodhead Publishing, 2017, pp. 493–547, https://doi.org/10.1016/B978-0-08-100662-7.00008-7.
[22] G.S. Stelling, S.P.A. Duinmeijer, A staggered conservative scheme for every Froude number in rapidly varied shallow water flows, Int. J. Numer. Methods Fluid. 43 (2003) 1329–1354, https://doi.org/10.1002/fld.537.
[23] L. Zou, H. Zhao, H. Zhang, New analytical solutions to the two-phase water faucet problem, Prog. Nucl. Energy 91 (2016) 389–398, https://doi.org/10.1016/j.pnucene.2016.05.013.
[24] R. Courant, K. Friedrichs, H. Lewy, On the partial difference equations of mathematical physics, IBM J. Res. Dev. 11 (1967) 215–234, https://doi.org/10.1147/rd.112.0215.
[25] G.F. Hewitt, J.M. Delhaye, N. Zuber, Multiphase Science and Technology, Hemisphere Publishing Co, New York, 1986, https://doi.org/10.1007/978-3-662-01657-2.